ACS APPLIED MATERIALS & INTERFACES

Research Article

www.acsami.org

Three-Dimensional Co_3O_4@$NiMoO_4$ Core/Shell Nanowire Arrays on Ni Foam for Electrochemical Energy Storage

Daoping Cai, Dandan Wang, Bin Liu, Lingling Wang, Yuan Liu, Han Li, Yanrong Wang, Qiuhong Li, and Taihong Wang*

Pen−Tung Sah Institute of Micro−Nano Science and Technology, Xiamen University, Xiamen 361000, People's Republic of China

Supporting Information

ABSTRACT: In this work, we report a facile two-step hydrothermal method to synthesize the unique three-dimensional Co_3O_4@$NiMoO_4$ core/shell nanowire arrays (NWAs) on Ni foam for the first time. The Co_3O_4 nanowires are fully covered by ultrathin mesoporous $NiMoO_4$ nanosheets. When evaluated as a binder-free electrode for supercapacitors in a 2 M KOH aqueous solution, the Co_3O_4@$NiMoO_4$ hybrid electrode exhibits a greatly enhanced areal capacitance of 5.69 F cm^{-2} at a high current density of 30 mA cm^{-2}, nearly 5 times that of the pristine Co_3O_4 electrode (1.10 F cm^{-2}). The energy density of the hybrid electrode is 56.9 W h kg^{-1} at a high power density of 5000 W kg^{-1}. In addition, the Co_3O_4@$NiMoO_4$ hybrid electrode also exhibits good rate capability and cycling stability, which would hold great promise for electrochemical energy storage.

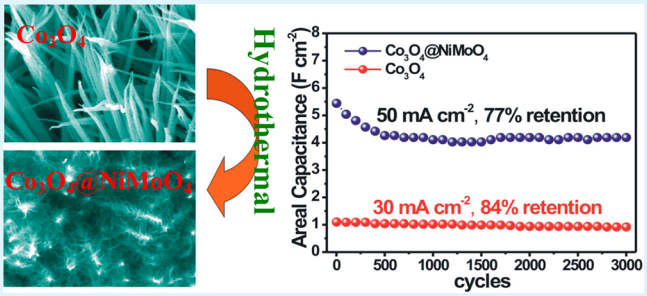

KEYWORDS: *nickel molybdate, core/shell, electrode material, Ni foam, hydrothermal method, supercapacitors*

1. INTRODUCTION

The development of efficient energy storage systems is an emerging requirement to meet the needs of modern society and ecological concerns.[1−3] Lithium-ion batteries (LIBs) and supercapacitors (SCs), as two major devices for electrochemical energy storage, have been receiving worldwide attention because of their vital roles in our daily lives.[4,5] Compared with LIBs, SCs are superior in the areas of high power density, fast charge/discharge processes, long lifespan, environmental friendliness, and safety.[6,7] SCs, also called electrochemical capacitors, are usually grouped into two categories: electrical double-layer capacitors (EDLCs) and pseudocapacitors.[8,9] Carbonaceous materials are typical electrode materials for EDLCs, and metal oxides/hydroxides and conducting polymers are typical electrode materials for pseudocapacitors.[10,11] In general, pseudocapacitance is much higher than electrical double-layer capacitance because of their fast and reversible faradic redox reactions. RuO_2 is one of the most notable pseudocapacitive materials, but the expensive nature and toxicity of ruthenium exclude it from wide application.[12−14] Cobalt oxide, because of its high theoretical specific capacitance, low cost, and environmentally friendly nature, is generally considered as a promising electrode material for pseudocapacitors.[15−18] Currently, tremendous efforts have been devoted to combining the unique properties of individual constituents to further improve their electrochemical performance.[19−22] For examples, Liu et al. reported the unique Co_3O_4@MnO_2 hybrid nanowire arrays (NWAs), which exhibited a high capacitance (4−10-fold increase in the areal capacitance with respect to a pristine Co_3O_4 array) with good cycle performance.[21] Zhou et al. reported a three-dimensional (3D) CoO@PPy hybrid NWA on Ni foam with outstanding pseudocapacitive performance that exhibited a much higher areal capacitance of 4.43 F cm^{-2} at 1 mA cm^{-2}, nearly 4 times that of the pristine CoO nanowire electrode (1.23 F cm^{-2}).[22]

Metal molybdates, especially $NiMoO_4$, have attracted great research interest because of their excellent electrochemical performance, low cost, and environmental friendliness.[23−25] It is well-accepted that large specific area and high electrical conductivity can lead to excellent performance for SC applications.[17,20,22] The binary metal oxide $NiMoO_4$ has been reported to exhibit high electrical conductivity of about 10^{-6} S cm^{-1}, which is much higher than that of the single-component metal oxide NiO.[26] It has been proven that the main function of the Mo element is to improve the conductivity of metal molybdates, and it does not participate in any redox reaction.[27] However, it is still a big challenge to synthesize a $NiMoO_4$ nanomaterial with large specific area and high electrical conductivity for SC applications. Recently, we synthesized ultrathin mesoporous $NiMoO_4$ nanosheets with large surface area (107.4 m^2 g^{-1}), which exhibited an ultrahigh specific capacitance of 1654.9 F g^{-1} at a current density of 2 A g^{-1}.[28] On the basis of the above consideration, in this work, we successfully develop a facile and efficient hydrothermal method to construct a unique Co_3O_4@$NiMoO_4$ hybrid nanostructure on Ni foam by growing ultrathin mesoporous $NiMoO_4$

Received: January 8, 2014
Accepted: March 5, 2014
Published: March 5, 2014

   dx.doi.org/10.1021/am500060m | ACS Appl. Mater. Interfaces 2014, 6, 5050−5055

nanosheets on Co_3O_4 NWAs. To the best of our knowledge, such a unique Co_3O_4@$NiMoO_4$ hybrid nanostructure has never been reported before. Benefiting from the multiple apparent advantages of the NWA configuration, such as high surface area, short ion diffusion path, and direct growth on a conductive substrate, the as-prepared Co_3O_4@$NiMoO_4$ hybrid electrode exhibits remarkable electrochemical performance with high capacitance, good rate capability, and desirable life cycle at high current density.

2. EXPERIMENTAL SECTION

2.1. Material Synthesis. All of the reagents used in the experiment were of analytical grade and were used without further purification. Prior to the synthesis, the Ni foam ($2 \times 1 \times 0.1$ cm^3) was cleaned by sonication in acetone, ethanol, and deionized (DI) water in sequence for 10 min each.

Synthesis of Co_3O_4 NWAs. The Co_3O_4 NWAs growing on Ni foam were from the literature.[22,29] In a typical synthesis, 0.727 g of $Co(NO_3)_2 \cdot 6H_2O$ and 0.7 g of urea were dissolved in 35 mL of DI water under constant magnetic stirring. The solution was transferred to a 50 mL Teflon-lined stainless steel autoclave, with a piece of pretreated Ni foam immersed in the reaction solution. The autoclave was sealed and maintained at 95 °C for 8 h and then cooled to room temperature. The array sample was collected and rinsed with distilled water several times, followed by annealing at 400 °C in air for 3 h.

Synthesis of Co_3O_4@$NiMoO_4$ Hybrid NWAs.[28] In a typical synthesis, 1 mmol of $Ni(CH_3COO)_2 \cdot 4H_2O$, 0.2 g of $(NH_4)_6Mo_7O_{24} \cdot 4H_2O$, and 0.24 g of urea were dissolved into 10.0 mL of DI water. The mixture was subjected to an intense ultrasonic treatment for a few minutes in order to form a light-green solution and then transferred to a 25 mL Teflon-lined stainless steel autoclave. Afterward, a piece of the Co_3O_4 NWA supported Ni foam was immersed in the reaction solution. The autoclave was sealed and maintained at 160 °C for 1 h and then cooled to room temperature. The array sample was taken out and rinsed with distilled water and alcohol several times, followed by annealing at 400 °C in air for 2 h.

2.2. Material Characterization. The powder X-ray diffraction (XRD) patterns were recorded on a Panalytical X-pert diffractometer with Cu Kα radiation. The morphology and crystal structure were observed by scanning electron microscopy (SEM; Hitachi S4800) and high-resolution transmission electron microscopy (HRTEM; JEM-2100) with an acceleration voltage of 200 kV.

2.3. Electrochemical Measurements. The electrochemical measurements were carried out in a three-electrode electrochemical cell containing a 2 M KOH aqueous solution as the electrolyte. The Co_3O_4 NWAs and Co_3O_4@$NiMoO_4$ hybrid NWAs were directly used as the working electrodes. The area of the working electrode immersed in the electrolyte was controlled to about 1 cm^2. The mass loading of Co_3O_4 on Ni foam was around 2.4 mg cm^{-2}, and the mass loading of $NiMoO_4$ on Co_3O_4/Ni foam was around 2.8 mg cm^{-2}, respectively. The electrochemical measurements were conducted with a CHI660E electrochemical workstation. A standard calomel electrode was used as the reference electrode and Pt foil as the counter electrode, and all of the experiments were done at ambient temperature. Electrochemical impedance spectroscopy (EIS) measurements were performed by applying an alternating-current voltage with 5 mV amplitude in a frequency range from 0.01 Hz to 100 kHz. The specific capacitance (C) and areal capacitance were calculated according to following equations:[16,21]

$$C = \frac{It}{mV} \quad \text{and} \quad C = \frac{It}{SV} \tag{1}$$

where I is the constant discharge current (A), t is the discharge time (s), V is the potential window (V), m is the total mass (g) of the electrode material on Ni foam, and S is the geometrical area (cm^2) of the working electrode.

3. RESULTS AND DISCUSSION

3.1. Synthesis and Characterization. The unique Co_3O_4@$NiMoO_4$ core/shell nanostructure is synthesized through a facile two-step hydrothermal method. Figure 1 shows typical SEM images of the Co_3O_4 NWAs on Ni foam under different magnifications. The Ni foam is covered by a large number of Co_3O_4 nanowires (Figure 1A,B). The magnified image (Figure 1C) reveals that they are highly porous, which is due to the release of gases during the calcination process.[29,30] The aligned Co_3O_4 nanowires with an average diameter of 70 nm are adequately separated. Figure 1D shows an SEM image of the Co_3O_4 NWAs from the side view, and their height is about 3 μm. The composition of the Co_3O_4 NWAs was studied by XRD. As shown in Figure S1 in the Supporting Information, two typical peaks in the XRD pattern of Co_3O_4 are well indexed to the (311) and (440) planes of Co_3O_4 (JCPDS card 42-1467), which is consistent with the literature.[15,19]

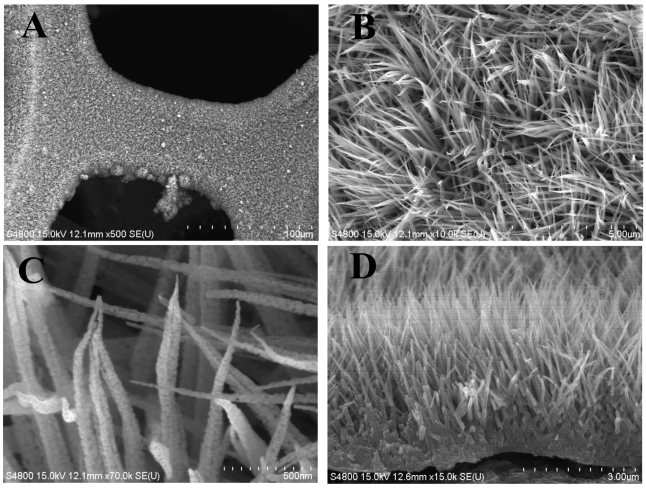

Figure 1. (A–C) Typical SEM images of the Co_3O_4 NWAs on Ni foam at different magnifications. (D) Co_3O_4 NWAs from the side view.

Afterward, the Co_3O_4 NWAs on Ni foam serve as the backbone for subsequent hydrothermal growth of the ultrathin mesoporous $NiMoO_4$ nanosheets. Figure 2 shows typical SEM images of the Co_3O_4@$NiMoO_4$ core/shell NWAs on Ni foam under different magnifications. It is worth noting that the uniformity of the nanostructure is still well retained (Figure 2A,B). The core/shell nanostructure can be easily distinguished from the magnified image (Figure 2C). The $NiMoO_4$ nanosheets show folding silk-like morphology with a transparent feature, suggesting the ultrathin nature. Impressively, the Co_3O_4 NWAs can provide a vast number of sites for the growth of ultrathin $NiMoO_4$ nanosheets, leading to a large increase of the surface area. The $NiMoO_4$ nanosheets are interconnected with each other, which creates loose porous nanostructures with abundant open space for ion diffusion within the electrode.[31] Obviously, the Co_3O_4 nanowires are uniformly covered by the $NiMoO_4$ nanosheets from the root to the tip, as observed from the side view in Figure 2D. Because of the low crystallinity of these $NiMoO_4$ nanosheets, the Co_3O_4@$NiMoO_4$ core/shell nanowires were scratched down from Ni foam and studied by XRD. As shown in Figure S1 in the Supporting Information, apart from the peaks from Co_3O_4

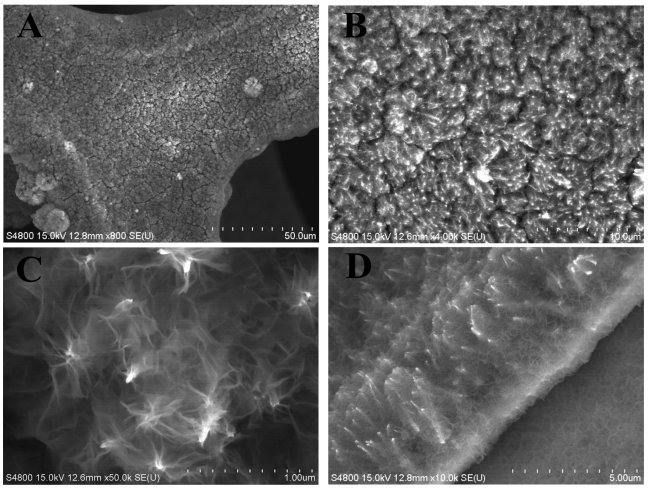

Figure 2. (A–C) Typical SEM images of the Co_3O_4@$NiMoO_4$ core/shell NWAs on Ni foam at different magnifications. (D) Co_3O_4@$NiMoO_4$ core/shell NWAs from the side view.

(JCPDS card 42-1467), we do observe some new peaks in the XRD pattern of the Co_3O_4@$NiMoO_4$ core/shell nanowires. According to our previous work, these new peaks could be indexed to $NiMoO_4$ (JCPDS card 45-0142).[28] The probable reason for such a weak signal is attributed to the low crystallinity and ultrathin features of the $NiMoO_4$ nanosheets.

The structural and morphological properties of the Co_3O_4 and Co_3O_4@$NiMoO_4$ core/shell nanowire were characterized by transmission electron microscopy (TEM). As shown in Figure 3A, the highly porous structure of the Co_3O_4 nanowire is also confirmed by the TEM image. The rings in the selected-area electron diffraction (SAED) pattern can be indexed as the

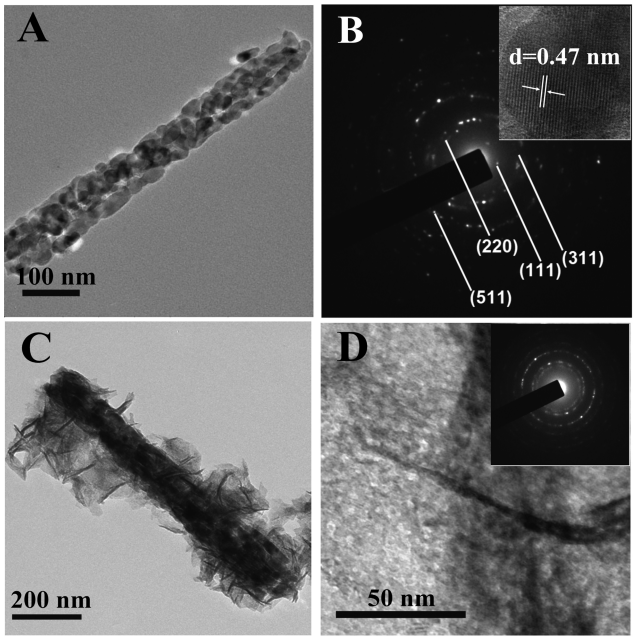

Figure 3. (A) Typical TEM image of an individual Co_3O_4 nanowire. (B) Corresponding SAED pattern (with the inset showing the HRTEM image). (C) typical TEM image of an individual Co_3O_4@$NiMoO_4$ core/shell structure. (D) Observation of the mesoporous feature (with the inset showing the SAED pattern taken from the shell region).

(111), (220), (311), and (511) planes of the the cubic structure Co_3O_4 (JCPDS card 42-1467), respectively, which is consistent with the XRD results, as shown in Figure 3B. From the HRTEM image, the lattice fringes can be readily indexed to the (111) crystal planes of Co_3O_4. Figure 3C shows the typical TEM image of an individual Co_3O_4@$NiMoO_4$ core/shell nanostructure. The TEM image also confirms the unique core/shell nanostructure. The surface of the porous Co_3O_4 nanowire is fully wrapped by the ultrathin $NiMoO_4$ nanosheets. Numerous mesopores (about 5–10 nm) are uniformly distributed throughout the whole surface of the nanosheets (Figure 3D). It is well-accepted that the mesoporous structure will not only greatly increase the electrode/electrolyte contact area but also facilitate mass transport of the electrolytes within the electrodes.[17,31] The well-defined diffraction rings in the SAED pattern (inset in Figure 3D) indicate the polycrystalline nature of the ultrathin $NiMoO_4$ nanosheets. Furthermore, energy-dispersive spectrometry (EDS) analysis reveals the elements of Co in the core region and Mo and Ni in the shell region. The signal of Cu is from the copper grid (Figure S2 in the Supporting Information).

3.2. Electrochemical Investigation. In order to highlight the merits of our electrode design, both of the Co_3O_4 and Co_3O_4@$NiMoO_4$ hybrid NWAs were evaluated as binder-free electrodes for SCs in a 2 M KOH aqueous solution. Figure 4

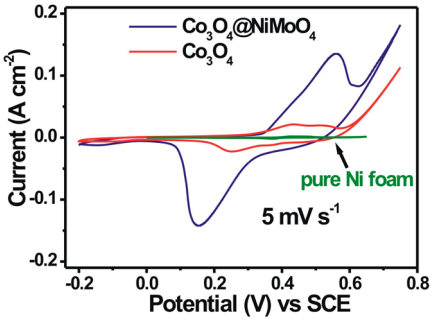

Figure 4. CV curves of the Co_3O_4 and Co_3O_4@$NiMoO_4$ hybrid electrodes at a scan rate of 5 mV s^{-1}.

shows the typical cyclic voltammetry (CV) curves of the Co_3O_4 and Co_3O_4@$NiMoO_4$ hybrid electrodes at a scan rate of 5 mV s^{-1}. Two pairs of redox peaks are observed for the Co_3O_4 electrode, which is due to the Co^{2+}/Co^{3+} and Co^{3+}/Co^{4+} reactions.[16,32] For the hybrid electrode, the expanded peaks are mainly attributed to the Ni^{2+}/Ni^{3+} reaction.[27,33] The CV-integrated area of pure Ni foam is almost negligible compared with that of the Co_3O_4 and Co_3O_4@$NiMoO_4$ hybrid electrodes, revealing the almost no capacitance contribution of the current collector. Remarkably, the CV-integrated area of the hybrid electrode is much larger than that of the Co_3O_4 electrode, indicating a significant increase of the areal capacitance. The four peaks of the pristine Co_3O_4 electrode are almost encompassed by the Co_3O_4@$NiMoO_4$ hybrid electrode, indicating that the inside Co_3O_4 nanowire is not blocked from participating in the Faradaic reaction despite the $NiMO_4$ covering.[21,33]

The typical CV curves of the Co_3O_4@$NiMoO_4$ hybrid electrode at various scan rates are shown in Figure 5A. As the scan rate increases, the cathodic peak position shifts to a lower potential, which is attributed to the polarization effect of the electrode.[34] Figure 5B shows the charge/discharge curves of the

dx.doi.org/10.1021/am500060m | ACS Appl. Mater. Interfaces 2014, 6, 5050–5055

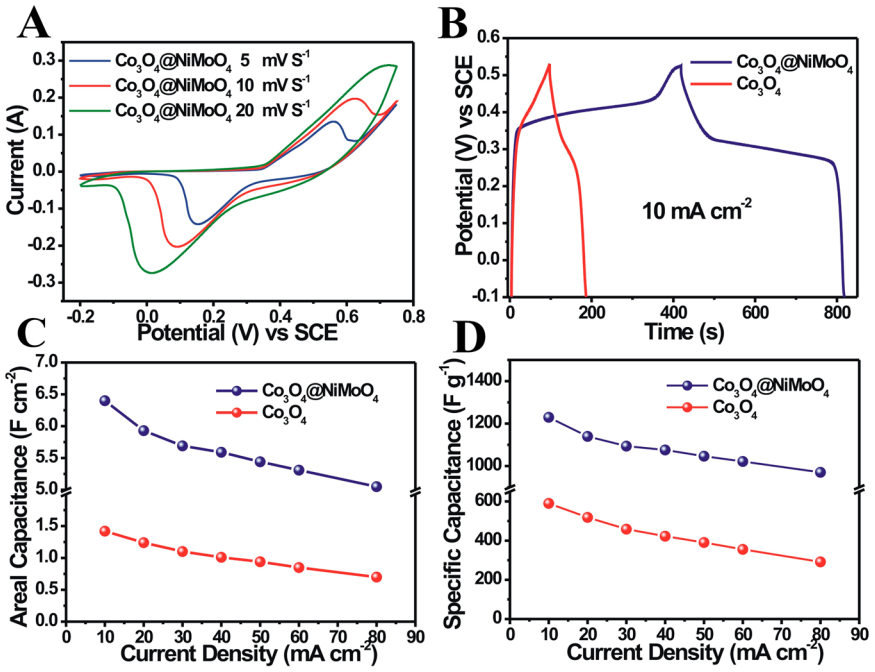

Figure 5. (A) CV curves of the Co_3O_4@$NiMoO_4$ hybrid electrode at various scan rates. (B) Charge/discharge curves of the Co_3O_4 and Co_3O_4@$NiMoO_4$ hybrid electrodes at a current density of 10 mA cm^{-2}. (C) Areal capacitances at different current densities. (D) Specific capacitances at different current densities (based on the total mass of the electrode materials on Ni foam).

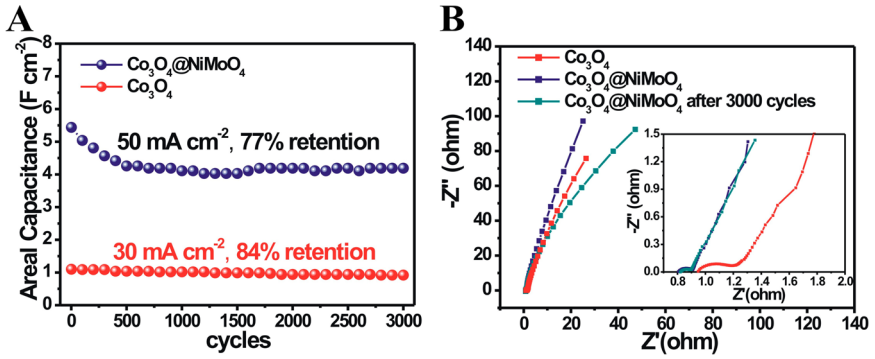

Figure 6. (A) Long-term cycling stability of the Co_3O_4 and Co_3O_4@$NiMoO_4$ hybrid electrodes. (B) Impedance Nyquist plots of the Co_3O_4 electrode and the Co_3O_4@$NiMoO_4$ hybrid electrode before and after 3000 cycles.

Co_3O_4 and Co_3O_4@$NiMoO_4$ hybrid electrodes at a current density of 10 mA cm^{-2}. Evidently, the Co_3O_4@$NiMoO_4$ hybrid electrode delivers higher areal capacitance than the Co_3O_4 electrode. Parts C and D of Figure 5 show the areal and specific capacitances of the Co_3O_4 and Co_3O_4@$NiMoO_4$ hybrid electrodes at different densities ranging from 10 to 80 mA cm^{-2}. On the basis of the above equations (the detailed specific capacitance calculation is described in the Supporting Information), the areal capacitances of the pristine Co_3O_4 electrode are calculated to be 1.42, 1.24, 1.10, 1.01, 0.94, 0.85, and 0.70 F cm^{-2}, and the specific capacitances are 590, 518, 459, 423, 391, 356, and 292 F g^{-1} at the current densities of 10, 20, 30, 40, 50, 60, and 80 mA cm^{-2}, respectively. Compared with the pristine Co_3O_4 electrode, the hybrid electrode exhibits significantly enhanced areal capacitances as high as 6.40, 5.93, 5.69, 5.59, 5.44, 5.31, and 5.05 F cm^{-2}, and the specific capacitances are 1230, 1140, 1094, 1076, 1046, 1022, and 970 F g^{-1} at the current densities of 10, 20, 30, 40, 50, 60, and 80 mA cm^{-2}, respectively. When the current density increases from 10 to 80 mA cm^{-2}, the capacitance retention of the hybrid electrode is about 79%, which is higher than of the pristine Co_3O_4 electrode (49%). This good rate capability is ascribed to the highly porous structure and the abundant space between the interconnected $NiMoO_4$ nanosheets, which can act as "ion-buffering reservoirs" for ions and thus shorten the diffusion distance from the external electrolyte to the interior surfaces.[35] It is worth mentioning that the results in this work are also higher than those in other previously reported core/shell nanoarchitectures, such as CoO@PPy hybrid NWAs (2.13 F cm^{-2} at 10 mA cm^{-2}),[22] Co_3O_4@NiO core/shell NWAs (1.35 F cm^{-2} at 6 mA cm^{-2}),[32] and $NiCo_2O_4$@MnO_2 core/shell NWAs (1.66 F cm^{-2} at 20 mA cm^{-2}).[36] Moreover, the hybrid electrode also delivers an impressive high energy density of 56.9 W h kg^{-1} at a high power density of 5000 W kg^{-1}, higher than the Co_3O_4 electrode of 25.7 W h kg^{-1} at 3969 W kg^{-1}.

The cycling stability plays a key role in SC applications. The long-term cycling stabilities of the Co_3O_4 and Co_3O_4@$NiMoO_4$ hybrid electrodes are shown in Figure 6A. The pristine Co_3O_4 electrode displays an areal capacitance of 0.92 F

dx.doi.org/10.1021/am500060m | ACS Appl. Mater. Interfaces 2014, 6, 5050−5055

cm^{-2} (~84% capacitance retention) after 3000 cycles at a current density of 30 mA cm^{-2}. Impressively, even with cycling at a higher current density of 50 mA cm^{-2}, the Co_3O_4@$NiMoO_4$ hybrid electrode still exhibits a high areal capacitance of 4.19 F cm^{-2} (~77% capacitance retention) after 3000 cycles. Capacitance fading occurs within the initial 500 cycles and then becomes stable from the 500 to 3000 cycles, which is similar to previous reports.[24,28] It is worth mentioning that the cycling stability of the Co_3O_4@$NiMoO_4$ hybrid electrode is better than that of other reported results, such as ZnO@Ni_3S_2 NWAs on Ni foam (42% capacitance retention after 2000 cycles at 10 A g^{-1}), Co_3O_4@$Ni(OH)_2$ NWAs on Ni foam (76% capacitance retention after 1000 cycles at 50 mA cm^{-2}), and $Ni(OH)_2$/$NiCo_2O_4$/CFP (36% capacitance retention after 1000 cycles at 5 mA cm^{-2}).[37−39] In addition, EIS was further carried out to reveal the reason for the excellent electrochemical behavior of the Co_3O_4@$NiMoO_4$ hybrid electrode. Figure 6B shows the impedance Nyquist plots of the Co_3O_4 electrode and the Co_3O_4@$NiMoO_4$ hybrid electrode before and after 3000 cycles in the frequency range of 0.01−100 kHz. In a low-frequency area, the Co_3O_4@$NiMoO_4$ hybrid electrode has a more ideal straight line, indicating more efficient electrolyte and proton diffusion. This can be attributed to the ultrathin and mesoporous $NiMoO_4$ nanosheets with large surface area and abundant open space that have enhanced utilization of the electrode materials and the supply of OH^-.[33] Obviously, the Co_3O_4@$NiMoO_4$ hybrid electrode also exhibits low bulk resistance and also low charge-transfer resistance, demonstrating the high electrochemical activity of the Co_3O_4@$NiMoO_4$ hybrid electrode for energy storage.[40] After 3000 cycles, the impedance spectra of the Co_3O_4@$NiMoO_4$ hybrid electrode almost remain unchanged, indicating the good cycling stability.

On the basis of the above results, the Co_3O_4@$NiMoO_4$ core/shell NWAs on Ni foam would provide great potential as binder-free electrodes for SC applications. The superior electrochemical performance can be mainly attributed to their multiple merits: (1) both the core and shell materials are good pseudocapacitive materials, contributing to the total capacitance;[36,41] (2) the direct growth of Co_3O_4@$NiMoO_4$ core/shell NWAs on the current collector ensures good mechanical adhesion and electric connection of the active material to the current collector;[4,12,42] (3) this electrode design avoids the use of polymer binder and conducting additives, improving utilization of the electrode material;[17,33] (4) the Co_3O_4 nanowires provide a vast number of sites for the growth of ultrathin and mesoporous $NiMoO_4$ nanosheets, leading to a large increase of the surface area; (5) the porous structure and abundant space between the interconnected $NiMoO_4$ nanosheets can act as "ion-buffering reservoirs" for ions and thus shorten diffusion distance from the external electrolyte to the interior surfaces.[17,31]

4. CONCLUSIONS

In this work, 3D Co_3O_4@$NiMoO_4$ core/shell NWAs on Ni foam have been synthesized through a facile two-step hydrothermal method. The Co_3O_4@$NiMoO_4$ hybrid electrode exhibits good electrochemical performance, with a large areal capacitance of 5.69 F cm^{-2} (1094 F g^{-1}) at a high current density of 30 mA cm^{-2}. When the current density increases from 10 to 80 mA cm^{-2}, the capacitance retention is about 79%, indicating a good rate capability. Impressively, the Co_3O_4@$NiMoO_4$ hybrid electrode still exhibits a high areal capacitance of 4.19 F cm^{-2} (~77% capacitance retention) after 3000 cycles at a high current density of 50 mA cm^{-2}, suggesting good cycling stability. These results demonstrate that the Co_3O_4@$NiMoO_4$ core/shell NWAs would provide great potential for electrochemical energy storage.

■ ASSOCIATED CONTENT

Ⓢ Supporting Information

XRD and EDS characterization and specific capacitance calculation. This material is available free of charge via the Internet at http://pubs.acs.org.

■ AUTHOR INFORMATION

Corresponding Author

*E-mail: thwang@xmu.edu.cn. Tel.: +86-0592-2183063. Fax: +86-0592-2197196.

Notes

The authors declare no competing financial interest.

■ ACKNOWLEDGMENTS

This research was partly supported by the National Basic Research Program of China (Grant 2007CB310500) and the National Natural Science Foundation of China (Grant 61376073).

■ REFERENCES

(1) Arico, A. S.; Bruce, P.; Scrosati, B.; Tarascon, J. M.; Schalkwijk, W. V. Nanostructured materials for advanced energy conversion and storage devices. *Nat. Mater.* **2005**, *4*, 366−377.

(2) Huang, Y.; Liang, J.; Chen, Y. An Overview of the Applications of Graphene-Based Materials in Supercapacitors. *Small* **2012**, *8*, 1805−1834.

(3) Zhao, X.; Sanchez, B. M.; Dobson, P. J.; Grant, P. S. The role of nanomaterials in redox-based supercapacitors for next generation energy storage devices. *Nanoscale* **2011**, *3*, 839−855.

(4) Jiang, J.; Li, Y.; Liu, J.; Huang, X.; Yuan, C.; Lou, X. W. Recent Advances in Metal Oxide-based Electrode Architecture Design for Electrochemical Energy Storage. *Adv. Mater.* **2012**, *24*, 5166−5180.

(5) Simon, P.; Gogotsi, Y. Materials for electrochemical capacitors. *Nat. Mater.* **2008**, *7*, 845−854.

(6) Wang, Y.; Xia, Y. Recent Progress in Supercapacitors: From Materials Design to System Construction. *Adv. Mater.* **2013**, *25*, 5336−5342.

(7) Yuan, C. Z.; Gao, B.; Shen, L. F.; Yang, S. D.; Hao, L.; Lu, X. J.; Zhang, F.; Zhang, L. J.; Zhang, X. G. Hierarchically structured carbon-based composites: Design, synthesis and their application in electrochemical capacitors. *Nanoscale* **2011**, *3*, 529−545.

(8) Liu, C.; Li, F.; Ma, L. P.; Cheng, H. M. Advanced Materials for Energy Storage. *Adv. Mater.* **2010**, *22*, E28−E62.

(9) Choi, D.; Blomgren, G. E.; Kumta, P. N. Fast and Reversible Surface Redox Reaction in NanocrystallineVanadium Nitride Supercapacitors. *Adv. Mater.* **2006**, *18*, 1178−1182.

(10) Zhang, L. L.; Zhao, X. S. Carbon-based materials as supercapacitor electrodes. *Chem. Soc. Rev.* **2009**, *38*, 2520−2531.

(11) Wang, G.; Zhang, L.; Zhang, J. A review of electrode materials for electrochemical supercapacitors. *Chem. Soc. Rev.* **2012**, *41*, 797−828.

(12) Hu, C. C.; Chang, K. H.; Lin, M. C.; Wu, Y. T. Design and Tailoring of the Nanotubular Arrayed Architecture of Hydrous RuO_2 for Next Generation Supercapacitors. *Nano Lett.* **2006**, *6*, 2690−2695.

(13) Wu, Z. S.; Wang, D. W.; Ren, W.; Zhao, J.; Zhou, G.; Li, F.; Cheng, H. M. Anchoring Hydrous RuO_2 on Graphene Sheets for High-Performance Electrochemical Capacitors. *Adv. Funct. Mater.* **2010**, *20*, 3595−3602.

(14) Lin, K. M.; Chang, K. H.; Hu, C. C.; Li, Y. Y. Mesoporous RuO_2 for the next generation supercapacitors with an ultrahigh power density. *Electrochim. Acta* **2009**, *54*, 4574−4581.

(15) Xiong, S.; Yuan, C.; Zhang, X.; Xi, B.; Qian, Y. Shape-controlled synthesis of porous Co_3O_4 nanostructures for application in supercapacitors. *Chem.—Eur. J.* **2009**, *15*, 5320−5326.
(16) Meher, S. M.; Rao, G. R. Ultralayered Co_3O_4 for High-Performance Supercapacitor Applications. *J. Phys. Chem. C* **2011**, *115*, 15646−15654.
(17) Yuan, C.; Yang, L.; Hou, L.; Shen, L.; Zhang, X.; Lou, X. W. Growth of ultrathin mesoporous Co_3O_4 nanosheet arrays on Ni foam for high-performance electrochemical capacitors. *Energy Environ. Sci.* **2012**, *5*, 7883−7887.
(18) Xu, J.; Gao, L.; Gao, J.; Wang, W.; Chen, Z. Preparation and electrochemical capacitance of cobalt oxide (Co_3O_4) nanotubes as supercapacitor material. *Electrochim. Acta* **2010**, *56*, 732−736.
(19) Yan, J.; Wei, T.; Qiao, W.; Shao, B.; Zhao, Q.; Zhang, L.; Fan, Z. Rapid microwave-assisted synthesis of graphene nanosheet/Co_3O_4 composite for supercapacitors. *Electrochim. Acta* **2010**, *55*, 6973−6978.
(20) Yang, P.; Xiao, X.; Li, Y.; Ding, Y.; Qiang, P.; Tan, X.; Mai, W.; Lin, Z.; Wu, W.; Li, T.; Jin, H.; Liu, P.; Zhou, J.; Wong, C. P.; Wang, Z. L. Hydrogenated ZnO Core Shell Nanocables for Flexible Supercapacitors and Self-Powered Systems. *ACS Nano* **2013**, *7*, 2617−2626.
(21) Liu, J.; Jiang, J.; Cheng, C.; Li, H.; Zhang, J.; Gong, H.; Fan, H. J. Co_3O_4 Nanowire@MnO_2 Ultrathin Nanosheet Core/Shell Arrays: A New Class of High-Performance Pseudocapacitive Materials. *Adv. Mater.* **2011**, *23*, 2076−2081.
(22) Zhou, C.; Zhang, Y.; Li, Y.; Liu, J. Construction of High-Capacitance 3D CoO@Polypyrrole Nanowire Array Electrode for Aqueous Asymmetric Supercapacitor. *Nano Lett.* **2013**, *13*, 2078−2085.
(23) Guo, D.; Zhang, P.; Zhang, H.; Yu, X.; Zhu, J.; Li, Q.; Wang, T. $NiMoO_4$ nanowires supported on Ni foam as novel advanced electrodes for supercapacitors. *J. Mater. Chem. A* **2013**, *1*, 9024−9027.
(24) Liu, M. C.; Kong, L. B.; Lu, C.; Ma, X. J.; Li, X. M.; Luo, Y. C.; Kang, L. Design and synthesis of $CoMoO_4$−$NiMoO_4{\cdot}xH_2O$ bundles with improved electrochemical properties for supercapacitors. *J. Mater. Chem. A* **2013**, *1*, 1380−1387.
(25) Liu, M. C.; Kang, L.; Kong, L. B.; Lu, C.; Ma, X. J.; Li, X. M.; Luo, Y. C. Facile synthesis of $NiMoO_4$. xH_2O nanorods as a positive electrode material for supercapacitors. *RSC Adv.* **2013**, *3*, 6472−6478.
(26) Moreno, B.; Chinarro, E.; Colomer, M. T.; Jurado, J. R. Combustion Synthesis and Electrical Behavior of Nanometric β-$NiMoO_4$. *J. Phys. Chem. C* **2010**, *114*, 4251−4257.
(27) Mai, L. Q.; Yang, F.; Zhao, Y. L.; Xu, X.; Xu, L.; Luo, Y. Z. Hierarchical $MnMoO_4$/$CoMoO_4$ heterostructured nanowires with enhanced supercapacitor performance. *Nat. Commun.* **2011**, *2*, 381−385.
(28) Cai, D.; Liu, B.; Wang, D.; Liu, Y.; Wang, L.; Li, H.; Wang, Y.; Wang, C.; Li, Q.; Wang, T. Facile hydrothermal synthesis of hierarchical ultrathin mesoporous $NiMoO_4$ nanosheets for high performance supercapacitors. *Electrochim. Acta* **2014**, *115*, 358−363.
(29) Jiang, J.; Liu, J.; Ding, R.; Ji, X.; Hu, Y.; Li, X.; Hu, A.; Wu, F.; Zhu, Z.; Huang, X. Direct Synthesis of CoO Porous Nanowire Arrays on Ti Substrate and Their Application as Lithium-Ion Battery Electrodes. *J. Phys. Chem. C* **2010**, *114*, 929−932.
(30) Li, J.; Zhao, W.; Huang, F.; Manivannan, A.; Wu, N. Single-crystalline $Ni(OH)_2$ and NiO nanoplatelet arrays as supercapacitor electrodes. *Nanoscale* **2011**, *3*, 5103−5109.
(31) Yuan, C.; Li, J.; Hou, L.; Zhang, X.; Shen, L.; Lou, X. W. Ultrathin Mesoporous $NiCo_2O_4$ Nanosheets Supported on Ni Foam as Advanced Electrodes for Supercapacitors. *Adv. Funct. Mater.* **2012**, *22*, 4592−4597.
(32) Xia, X.; Tu, J.; Zhang, Y.; Wang, X.; Gu, C.; Zhao, X. B.; Fan, H. J. High-Quality Metal Oxide Core/Shell Nanowire Arrays on Conductive Substrates for Electrochemical Energy Storage. *ACS Nano* **2012**, *6*, 5531−5538.
(33) Guan, C.; Liu, J.; Cheng, C.; Li, H.; Li, X.; Zhou, W.; Zhang, H.; Fan, H. J. Hybrid structure of cobalt monoxide nanowire@nickel hydroxidenitrate nanoflake aligned on nickel foam for high-rate supercapacitor. *Energy Environ. Sci.* **2011**, *4*, 4496−4499.
(34) Yan, J.; Fan, Z.; Sun, W.; Ning, C.; Wei, T.; Zhang, Q.; Zhang, R.; Zhi, L.; Wei, F. Advanced Asymmetric Supercapacitors Based on $Ni(OH)_2$/Graphene and Porous Graphene Electrodes with High Energy Density. *Adv. Funct. Mater.* **2012**, *22*, 2632−2641.
(35) Yuan, C.; Zhang, X.; Su, L.; Gao, B.; Shen, L. Facile synthesis and self-assembly of hierarchical porous NiO nano/micro spherical superstructures for high performance supercapacitors. *J. Mater. Chem.* **2009**, *19*, 5772−5777.
(36) Yu, L.; Zhang, G.; Yuan, C.; Lou, X. W. Hierarchical $NiCo_2O_4$@MnO_2 core−shell heterostructured nanowire arrays on Ni foam as high-performance supercapacitor electrodes. *Chem. Commun.* **2013**, *49*, 137−139.
(37) Xing, Z.; Chu, Q.; Ren, X.; Ge, C.; Qusti, A. H.; Asiri, A. M.; Al-Youbi, A. O.; Sun, X. Ni_3S_2 coated ZnO array for high-performance supercapacitors. *J. Power Sources* **2014**, *245*, 463−467.
(38) Tang, C. H.; Yin, X.; Gong, H. Superior Performance Asymmetric Supercapacitors Based on a Directly Grown Commercial Mass 3D Co_3O_4@$Ni(OH)_2$ Core−Shell Electrode. *ACS Appl. Mater. Interfaces* **2013**, *5*, 10574−10582.
(39) Huang, L.; Chen, D.; Ding, Y.; Wang, Z. L.; Zeng, Z.; Liu, M. Hybrid Composite $Ni(OH)_2$@$NiCo_2O_4$ Grown on Carbon Fiber Paper for High-Performance Supercapacitors. *ACS Appl. Mater. Interfaces* **2013**, *5*, 11159−11162.
(40) Wang, K. P.; Teng, H. Structural Feature and Double-Layer Capacitive Performance of Porous Carbon Powder Derived from Polyacrylonitrile-Based Carbon Fiber. *J. Electrochem. Soc.* **2007**, *154*, A993−A998.
(41) Jiang, H.; Li, C.; Sun, T.; Ma, J. High-performance supercapacitor material based on $Ni(OH)_2$ nanowire−MnO_2 nanoflakes core−shell nanostructures. *Chem. Commun.* **2012**, *48*, 2606−2608.
(42) Xia, X.; Zhu, C.; Luo, J.; Zeng, Z.; Guan, C.; Ng, C. F.; Zhang, H.; Fan, H. J. Synthesis of Free-Standing Metal Sulfide Nanoarrays via Anion Exchange Reaction and Their Electrochemical Energy Storage Application. *Small* **2014**, *10*, 766−773.